AD-A121 900 DEVELOPMENT OF FRACTURE MECHANICS CONCEPTS APPLICABLE 1/1
TO AIRCRAFT STRUCTURES(U) GEORGE WASHINGTON UNIV
WASHINGTON DC SCHOOL OF ENGINEERING AN.. H LIEBOWITZ
UNCLASSIFIED 05 NOV 81 N00019-79-C-0491 F/G 1/3 NL

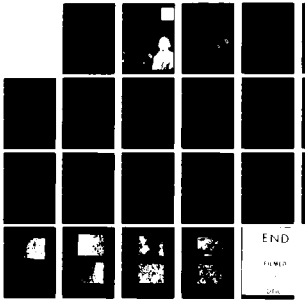

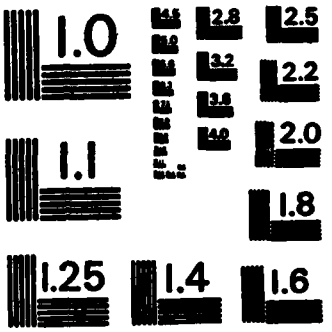

DEVELOPMENT OF FRACTURE MECHANICS CONCEPTS APPLICABLE TO AIRCRAFT STRUCTURES

THE GEORGE WASHINGTON UNIVERSITY

STUDENTS FACULTY STUDY R
ESEARCH DEVELOPMENT FUT
URE CAREER CREATIVITY CC
MMUNITY LEADERSHIP TECH
NOLOGY FRONTIE ESIGN
ENGINEERING APP ENC
GEORGE WASHIN NIV

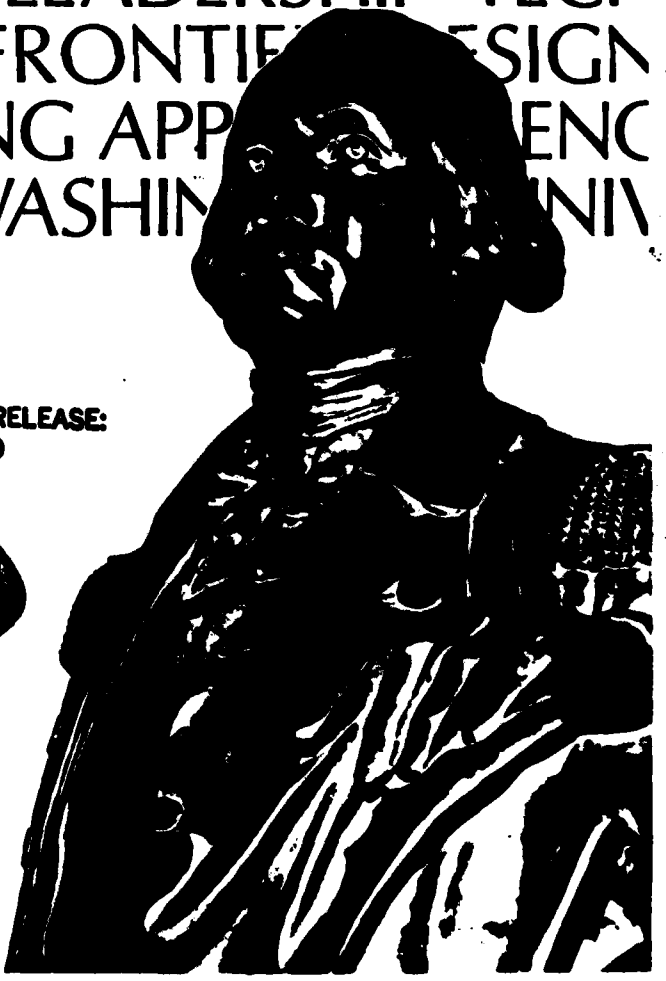

SCHOOL OF ENGINEERING
AND APPLIED SCIENCE

DEVELOPMENT OF FRACTURE MECHANICS CONCEPTS APPLICABLE TO AIRCRAFT STRUCTURES

Nov 5, 1981

NAVAIR Contract No. N00019-79-C-0491

Principal Investigator: H. Liebowitz

Final Scientific Report

School of Engineering and Applied Science
The George Washington University
Washington, D.C. 20052

In PART A of this report,

PREDICTION OF CONSTANT AMPLITUDE FATIGUE LIVES OF PRECRACKED SPECIMENS FROM ACCELERATED FATIGUE DATA

ABSTRACT

The feasibility of using an accelerated fatigue test program to predict constant amplitude fatigue lives of precracked specimens was examined. An analytical basis for the fracture mechanics approach was developed by modifying some earlier work that had been applied to unnotched specimens. A load program involving a linearly increasing load with the cycle number was used for the accelerated tests. The predicted curves from the accelerated test data were found to provide a good fit for the constant amplitude results in 2024-T3 and 7075-T6 aluminum alloys. These results indicate that the accelerated test data can be effectively employed to predict constant amplitude fatigue lives, while also providing a considerable reduction in testing time.

Cont'd

A-1

NOMENCLATURE

B - Constant in the equation of $\Delta\bar{K}_f$-N_d curve

C - Constant in the equation of $\Delta\bar{K}$-N curve

D - Coefficient in accelerated fatigue model

m - Exponent in the equation of $\Delta\bar{K}$-N curve

n - Number of cycles of constant $\Delta\bar{K}$ amplitude

N - Number of cycles to failure in constant $\Delta\bar{K}$ amplitude tests

N_d - Number of cycles causing structural damage in accelerated test

N_0 - Number of cycles that do not cause structural damage in accelerated test

N_f - Number of cycles to failure in accelerated test

p,r - Exponents in accelerated fatigue model

$\Delta\bar{K}$ - Stress intensity range in constant amplitude test

$\Delta\bar{K}_f$ - Stress intensity range at fracture in accelerated test

ΔK_{TH} - Threshold value of $\Delta\bar{K}$

$\Delta\bar{K}_\delta$ - Rate of increase of stress intensity range in an accelerated test

INTRODUCTION

Most service failures in machines and structural components are due to fatigue. Hence, considerable attention has been given to fatigue properties of materials. Most of the earlier experiments were performed on smooth specimens without cracks or other stress raisers. However, with the acceptance of fracture mechanics principles, a lot of studies have been made on precracked specimens with the emphasis of most tests placed on measurements of fatigue crack growth rates. Fatigue tests of both types are time-consuming and expensive, especially when the stress amplitude is low.

An attempt to reduce fatigue testing time was made by Prot [1] using an accelerated fatigue test method. He used this method to determine the endurance limit in completely reversed cycling of smooth specimens. A cyclic load, with the magnitude increasing linearly with cycle number, was used for the accelerated test. It was assumed that curves relating the fracture stress to the number of cycles to failure in constant amplitude tests and accelerated tests were hyperbolas, assymptotic to the endurance limit. This method was modified later by assuming that the curves were higher order hyperbolas [2,3]. Recently Basavaraju and Lim [4] improved this method by developing an analytical basis for predicting the entire constant amplitude S-N curve from accelerated test results. They obtained reasonably good agreement between the

predicted values and experimental results in completely reversed fatigue cycling of smooth specimens.

The accelerated test models assume that the cumulative damage (Miner's) rule is valid in all the stages of fatigue damage from crack initiation to final fracture. However, the damage accumulation processes in these stages are different, which could produce differences between the analytical predictions and experimental results. The number of cycles expended in crack initiation is very large, especially when the stress amplitude is low. In materials containing pre-existing cracks, the time for crack initiation is eliminated. Hence, the accelerated tests can be expected to yield better results with precracked specimens.

Another factor causing deviation from Miner's rule is the crack growth retardation or arrest when a high stress amplitude is followed by lower stress amplitudes. In accelerated testing the stress amplitude is increased in successive cycles, and hence, the difficulties associated with crack retardation or arrest are not encountered.

The purpose of this investigation was to examine the applicability of accelerated test methods to predict constant load amplitude lives of precracked specimens. This development is based on the stress intensity which is appropriate to precracked specimens rather than that based on stress. The analytical results are compared with experimental values obtained from testing 7075-T6 and 2024-T3 aluminum alloys.

ANALYTICAL BACKGROUND

The analytical approach used in this investigation is a modification of a recent paper by Basavaraju and Lim [4] which was based on the fatigue tests on unnotched specimens. In precracked specimens, although gross stress is proportional to the load, the stress distribution in the net cross sectional area changes continuously. A more accurate picture of the state of stress at the crack tip is given by the stress intensity factor, K. Hence, in this investigation the relations are developed in terms of the stress intensity factor. In constant load amplitude cycling the crack length changes continuously, but, in many practical situations, only the initial crack length is known. In these situations, the stress intensity values are calculated from the initial crack length and the applied load. The stress intensity factor based on the initial crack length is represented by $\bar{K}$.

In the accelerated tests the load amplitude (and stress intensity change, $\Delta\bar{K}$) increases linearly with the cycle number. Load cycling below a level known as the threshold value (ΔK_{TH}) is assumed to cause no structural damage. The test results permit the establishment of relations between $\Delta\bar{K}$ and N, the number of cycles to failure in a constant amplitude test, and $\Delta\bar{K}_f$ and N_d, the number of cycles causing damage in the accelerated tests. The $\Delta\bar{K}_f$-N_d curve in the

accelerated fatigue and $\Delta\bar{K}$-N curve in constant amplitude fatigue are assumed to be represented most effectively by higher order hyperbolas.

The hyperbolic equation for the constant amplitude test curve may be written as

$$(\Delta\bar{K}-\Delta\bar{K}_{TH})^{m} N = C \ , \tag{1}$$

where m and C are parameters determined by fitting Eqn. (1) to the experimental data. The hyperbola in the accelerated test may be expressed by the equation

$$(\Delta\bar{K}_f-\Delta\bar{K}_{TH})^{r} N_d = B \ , \tag{2}$$

where r and B serve the same functions in the accelerated tests as m and C. Since the increase in stress intensity per cycle, $\Delta\bar{K}_\delta$ is given by

$$\Delta\bar{K}_\delta = (\Delta\bar{K}_f-\Delta\bar{K}_{TH})/N_d \ , \tag{3}$$

the stress intensity range at fracture may be written as

$$\Delta\bar{K}_f = \Delta\bar{K}_{TH} + (B\ \Delta\bar{K}_\delta)^{\frac{1}{r+1}} \ . \tag{4}$$

Equation (4) may be rewritten as

$$\Delta\bar{K}_f = \Delta\bar{K}_{TH} + D\ (\Delta\bar{K}_\delta)^{p} \ , \tag{4a}$$

by the definition of new parameters D and p. If N_0 is

the number of cycles below ΔK_{TH}, the number of cycles causing fatigue damage, N_d is given by

$$N_d = N_f - N_0 = (\Delta\bar{K}_f - \Delta K_{TH})/\Delta\bar{K}_\delta \ . \qquad (5)$$

The first cycle causing fatigue damage has stress intensity range $\Delta K_{TH} + 1 \cdot \Delta\bar{K}_\delta$, the second cycle has stress intensity range $\Delta K_{TH} + 2 \cdot \Delta K_\delta$, the jth cycle has $\Delta K_{TH} + j \cdot \Delta K_\delta$ and so on with the stress intensity range becoming $\Delta K_{TH} + N_d \cdot \Delta\bar{K}_\delta$ for the last cycle. At each stress intensity level the fatigue life is given by Eqn. 1, but only one cycle is spent at each level. Hence, Miner's cumulative damage rule can be applied in the form

$$\frac{1}{N_1} + \frac{1}{N_2} + \frac{1}{N_3} \ldots \frac{1}{N_j} + \ldots \frac{1}{N_{N_d}} = 1 \ , \qquad (6)$$

where $N_j = \dfrac{C}{(\Delta\bar{K}_j - \Delta K_{TH})^m}$.

Since $\Delta\bar{K}_j = \Delta K_{TH} + j \cdot \Delta\bar{K}_\delta$,

$$N_j = \frac{C}{(j \cdot \Delta\bar{K}_\delta)^m} \ ,$$

and Eqn. (6) can be rewritten as

$$\frac{(\Delta\bar{K}_\delta)^m}{C} \left[1 + 2^m + 3^m + \ldots j^m + \ldots (N_d)^m\right] = 1 \ . \qquad (6a)$$

Basavaraju and Lim [4] have shown that Eqn. (6a) can be approximated by the form

$$\frac{(\Delta K_\delta)^m}{C} \quad \frac{N_d^{m+1}}{m+1} = 1 \ . \tag{7}$$

From any two accelerated test results, Eqn. (7) can be solved for m with the help of Eqn. (3) to obtain [4]

$$m = \frac{1 - p}{p} \ . \tag{8}$$

The constant C is given by

$$C = \frac{1}{m+1}(\Delta K_\delta)^m \ N_d^{m+1} = \frac{1}{m+1}(D)^{m+1} = pD^{1/p} \ . \tag{9}$$

If N_d and ΔK_δ are treated as continuous variables, Eqn. (8) can be obtained by differentiation of Eqn. (7) and substituting for N_d from Eqn. (3). Thus, from a knowledge of the constants, ΔK_{TH}, D and p in the accelerated test curve, the constants for the constant amplitude curve ΔK_{TH}, m and C can be determined and, hence, the complete curve can be obtained.

EXPERIMENTAL PROCEDURE

The experimental work for this research project was performed on two aluminum alloys, 2024-T3 and 7075-T6, using center-cracked sheet specimens shown in Fig. 1. Specimens with gauge length 27 in., width 12 in. and thickness 0.063 in. were tested in the L-T orientation. The crack length-to-width ratios (2a/w) for accelerated tests were 0.33 and 0.5 for 2024-T3 and 0.25 for 7075-T6. Constant amplitude lives were determined for various 2a/w ratios. The tests were performed on servohydraulic testing system. No antibuckling guides were used and the stress intensity ratio (R) was zero for all the tests.

The stress intensity increments for the accelerated tests were based on the fracture toughness (K_c). Hence, the fracture toughness values were first determined for these materials as a function of the crack length. It was found that the K_c values decreased with increasing crack length for both 2024-T3 (Fig. 2) and 7075-T6 (Fig. 3). The stress intensity increment for each accelerated test was chosen as a percentage of the K_c value corresponding to the given crack length.

RESULTS AND DISCUSSION

With the selection of the relatively brittle 7075-T6 and the more ductile 2024-T3 structural aluminum alloys for the experiments, it was possible to study the applicability of the accelerated test program to predict the constant amplitude lives of materials having considerable differences in ductility. Only one crack length-to-width ratio was studied for 7075-T6 while different ratios were examined for 2024-T3.

The values of the stress intensity factor range at fracture (ΔK_f) as a function of the number of cycles to failure (N_f) in the accelerated tests of 7075-T6 specimens with 2a/w = 0.25 are plotted in Fig. 4. A best-fit curve for these data in the form of Eqn. (4a) was obtained using the least squares method. For this curve values of the constants are: D = 114, p = 0.0606 and ΔK_{TH} = - 50 ksi$\sqrt{in}$. The predicted constant amplitude curve from these values has constants m = 15.502 and C = 5.306×10^{32}. The predicted curve and the experimental data are shown in Fig. 5. The agreement between the two is good, which verifies the validity of the accelerated test approach for a relatively brittle alloy.

The accelerated test data and the best-fit hyperbola for the 2024-T3 alloy with 2a/w = 0.5 are given in Fig. 6. The constants for this curve are: D = 94.0, p = 0.0645 and

ΔK_{TH} = - 34.6 ksi$\sqrt{in}$. The predicted constant amplitude curve has constants: m = 14.504 and C = 2.516 x 10^{29}. The predicted curve and the experimental data show excellent agreement, as indicated in Fig. 7. For the tests on 2024-T3 with 2a/w = 0.33, the best-fit curve has constants: D = 114.5, p = 0.057 and ΔK_{TH} = - 50 ksi$\sqrt{in}$., as shown in Fig. 8, and for the corresponding constant amplitude curve, m = 16.544 and C = 7.504 x 10^{34}. Here also the predicted curve and experimental data exhibit very good agreement, as seen in Fig. 9.

Constant amplitude tests were performed on 2024-T3 specimens of crack length-to-width ratio 0.4 and 0.6 as well. The constant amplitude test data for the four 2a/w values and the two constant amplitude curves predicted from the accelerated tests are plotted in Fig. 10. Although the values of the constants are somewhat different for the two curves, the actual results are in close agreement with each other. The difference in the position of the curves is thought to be due to the larger distance the crack must grow prior to fracture in the specimens having the smaller 2a/w values. The data points for 2a/w of 0.33 and 0.4 almost overlap, and those for 2a/w of 0.5 are very close to the prior two sets of data. The points for 2a/w of 0.6 are shifted to the left indicating that the remaining life for a given ΔK is less than predicted by the other results. This shows that accelerated tests using a single crack length-to-width ratio (2a/w) can be used

to predict constant load amplitude lives for different crack lengths, provided that the crack length remains small relative to the width of the specimen. Cracks having 2a/w higher than 0.5 are not of real practical importance because such a large portion of their useful lives would normally have already been expended.

The ΔK_{TH} obtained for both alloys have negative values. Such negative values for threshold stress intensity range are not realistic. Hence, these values should be considered only as constants for the curve and can be attributed to the shape of the ΔK-N curves, which are similar to the load (or stress) versus number of cycles curves for precracked specimens. In an earlier study, McEvily and Johnston [5] observed that in both 2024-T3 and 7075-T6 alloys the curves changed sharply from a high negative slope to a horizonal slope as they approached the threshold value. In the experiments conducted for the present program, the number of cycles to failure in constant amplitude test (N) did not exceed 10^6 cycles, with the greatest number of cycles to failure in accelerated test being approximately 10^5 cycles. Hence, the range of tests employed in this program did not provide data pertinent to the threshold values. However, in the ranges examined, the accelerated test results have been able to predict constant amplitude lives successfully, where the number of cycles and testing time were an order of magnitude lower than that required for constant amplitude tests.

CONCLUSIONS

A progressively increasing fatigue load program has been applied to predict the fatigue lives of precracked specimens in constant load amplitude cycling. The results show that this accelerated test program can predict the constant amplitude lives with good accuracy. Application of this approach will permit considerable reductions in the time and expense associated with the fatigue testing of materials containing flaws and other stress concentrations. Additional work is needed to determine the limits of applicability of the method, as well as its usefulness for other types of materials.

REFERENCES

1. E. M. Prot, "Fatigue Testing Under Progressive Loading, A New Technique for Testing Materials," Revue de Metallurgie, 1948, 45, pp. 481-489.
2. H. T. Corten, T. Dimoff and T. S. Dolan, "An Appraisal of the Prot Method of Fatigue Testing," Proc. ASTM, 1954, 54, pp. 875-902.
3. J. M. Diez and R. V. Salkin, "Appraisal of the Locati and Prot Methods for Determining Fatigue Limits," J. Materials, 1972, 7 (1), pp. 32-37.
4. C. Basavaraju and C. K. Lim, "An Analytical Approach to Determine Conventional S-N Curves from Accelerated-fatigue Data," Experimental Mechanics, 1977, pp. 375-380.
5. A. J. McEvily and T. L. Johnston, "The Role of Cross-Slip in Brittle Fracture and Fatigue," Proc. Internat. Conf. on Fracture, Sendai, Japan, 1965, pp. 515-546.

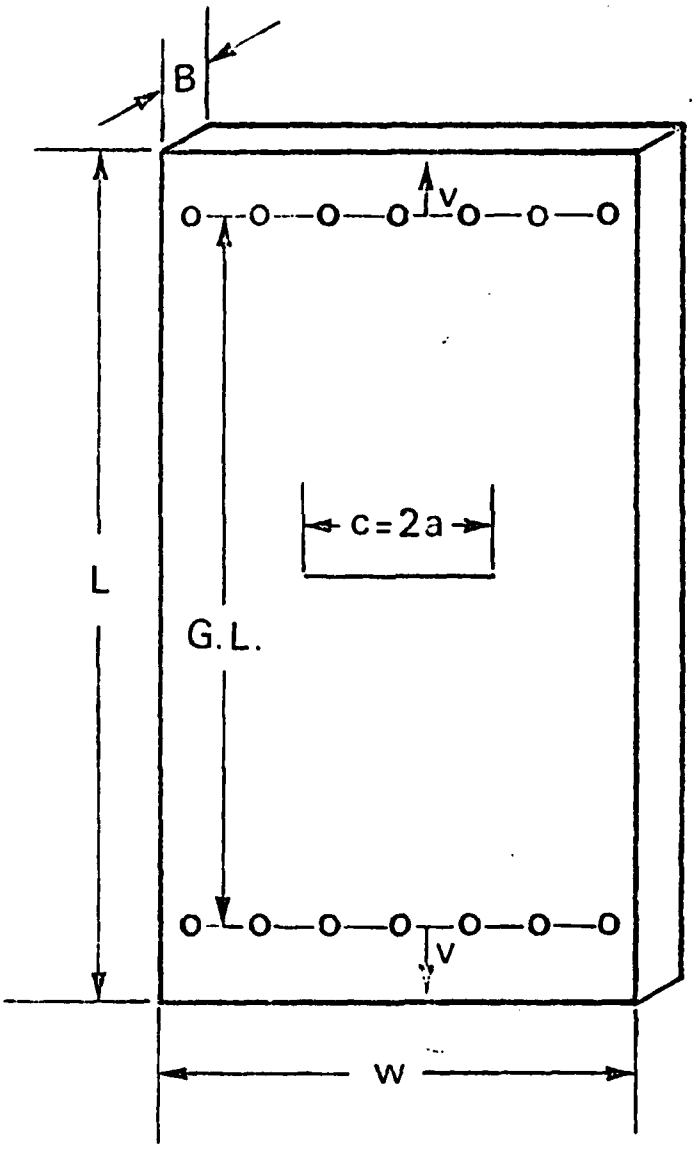

Fig. 1. General specimen geometry

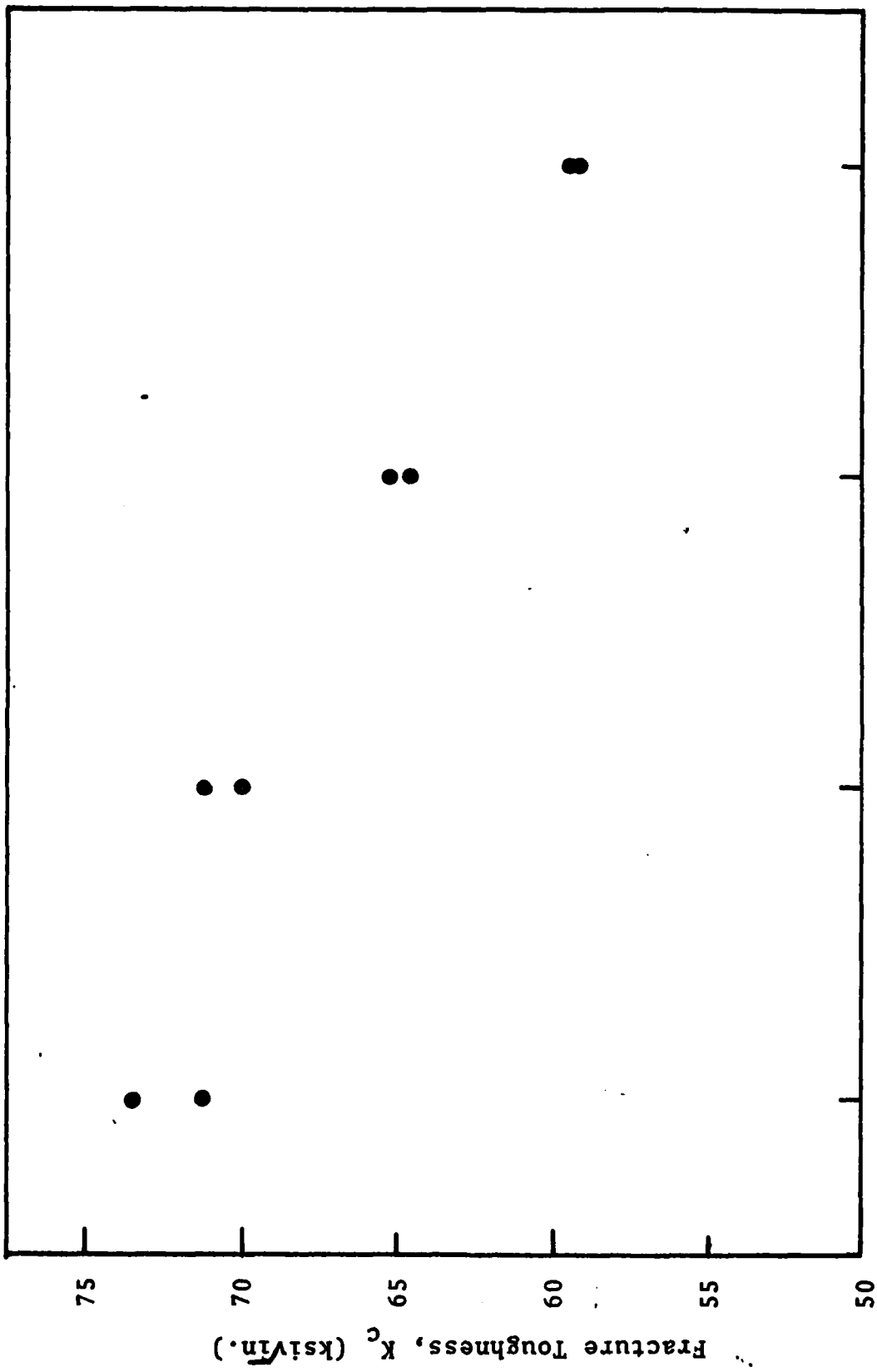

Fig. 2. Variation of fracture toughness with crack length-to width ratio in 2024-T3 alloy.

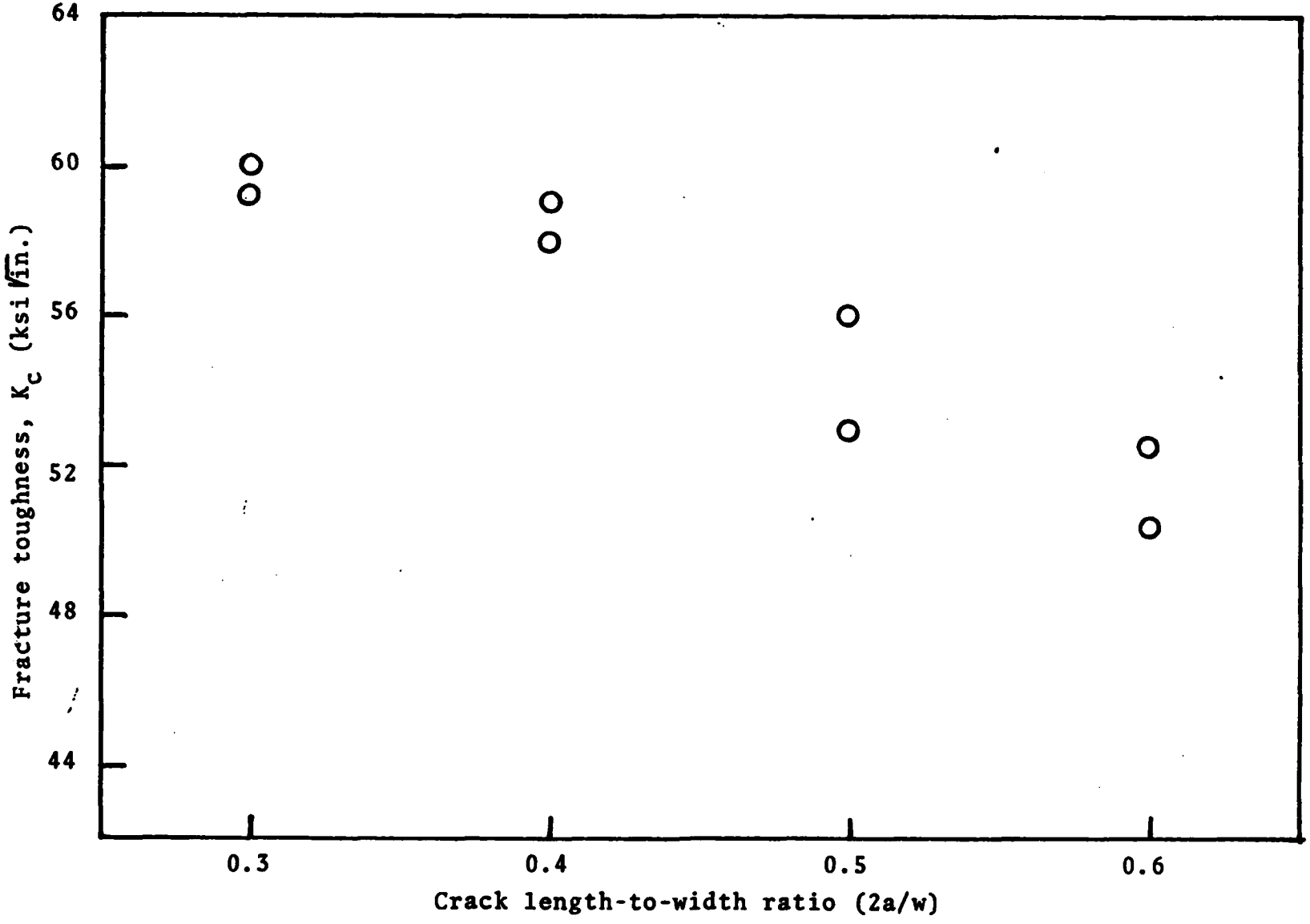

Fig. 3. Variation of fracture toughness with crack length-to-width ratio in 7075-T6 alloy.

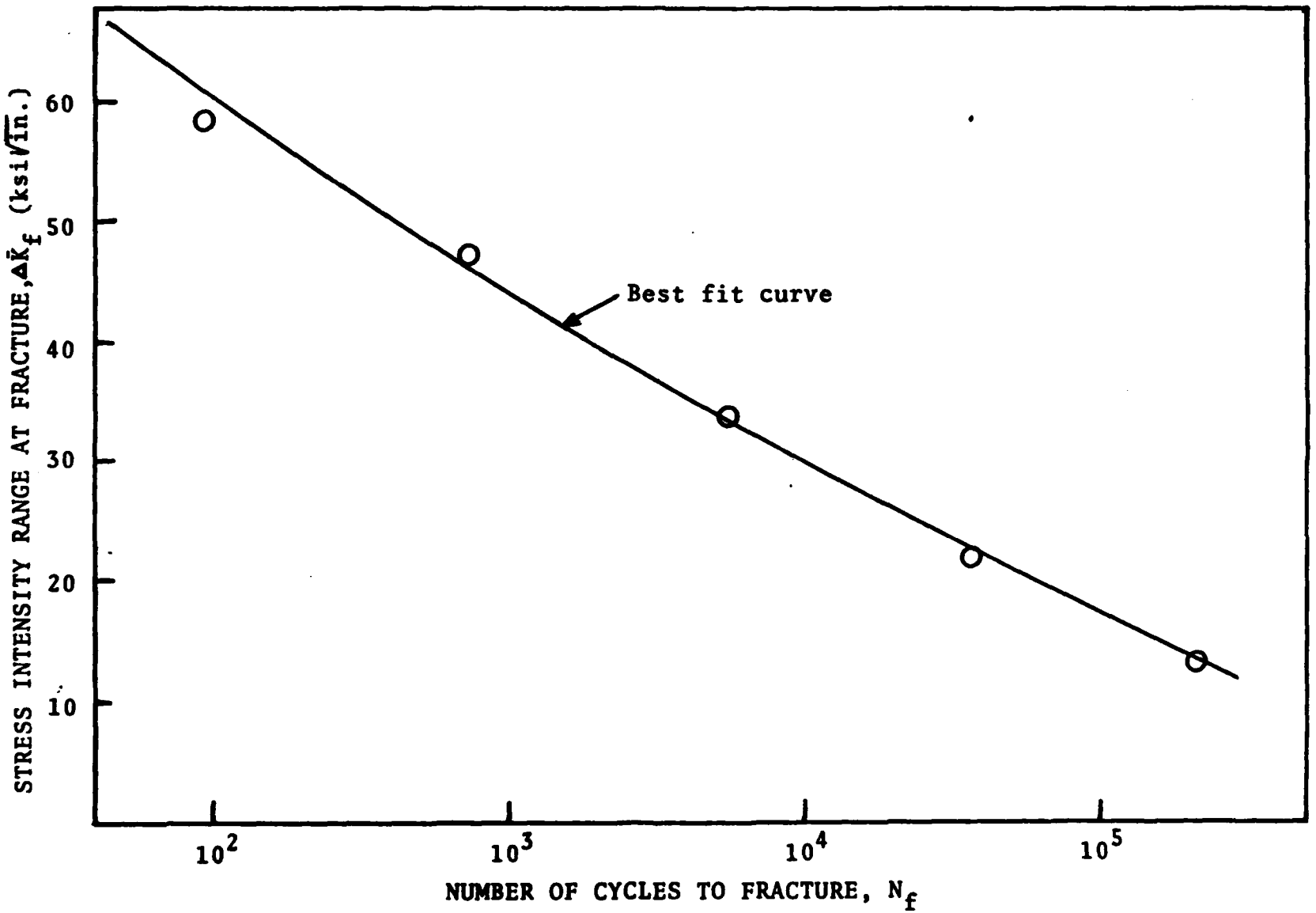

Fig. 4. Variation of stress intensity range at fracture with number of cycles to fracture in accelerated test of 7075-T6 alloy.

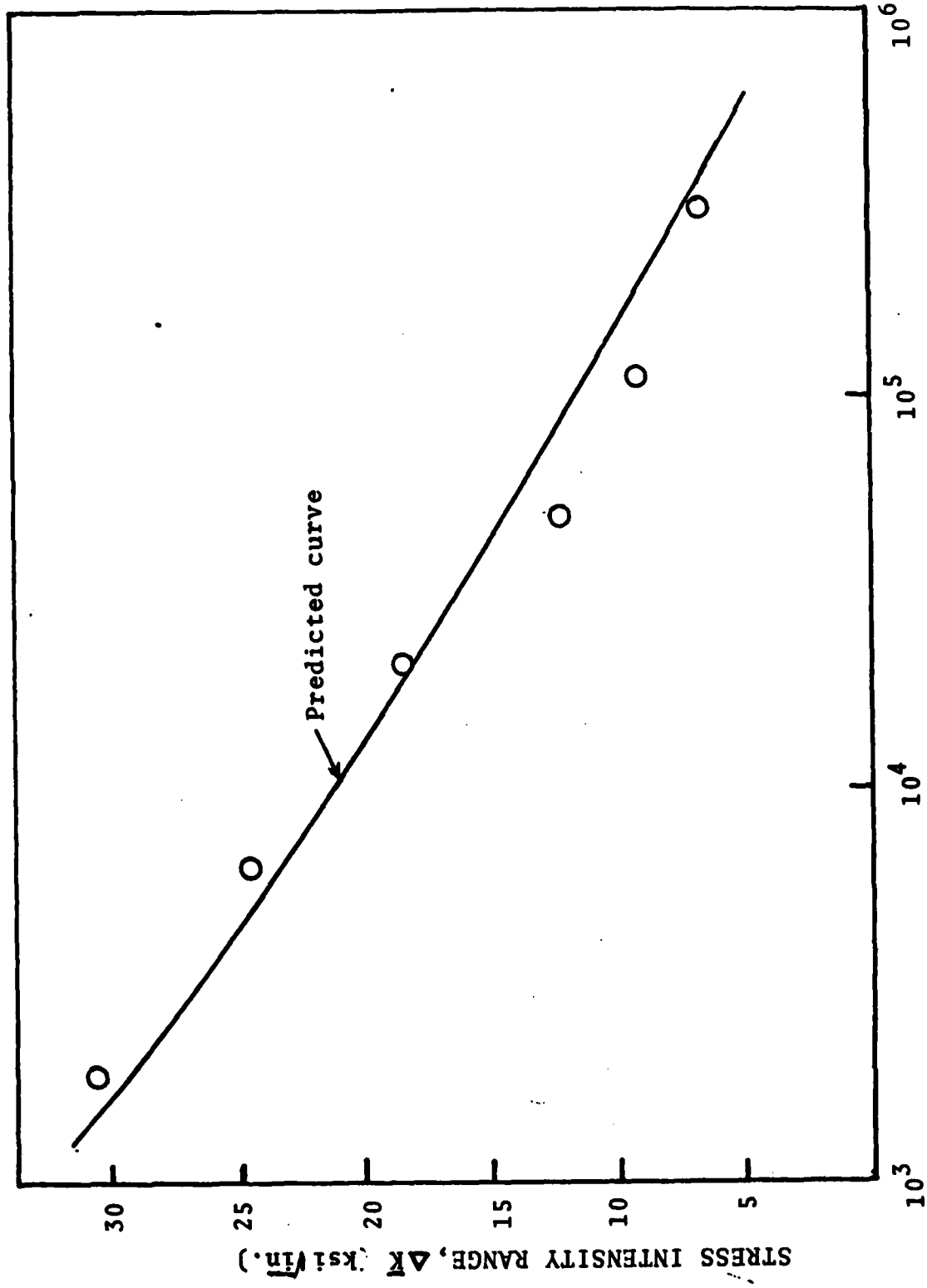

Fig. 5. Variation of stress intensity range with fatigue life in constant amplitude test of 7075-T6 alloy.

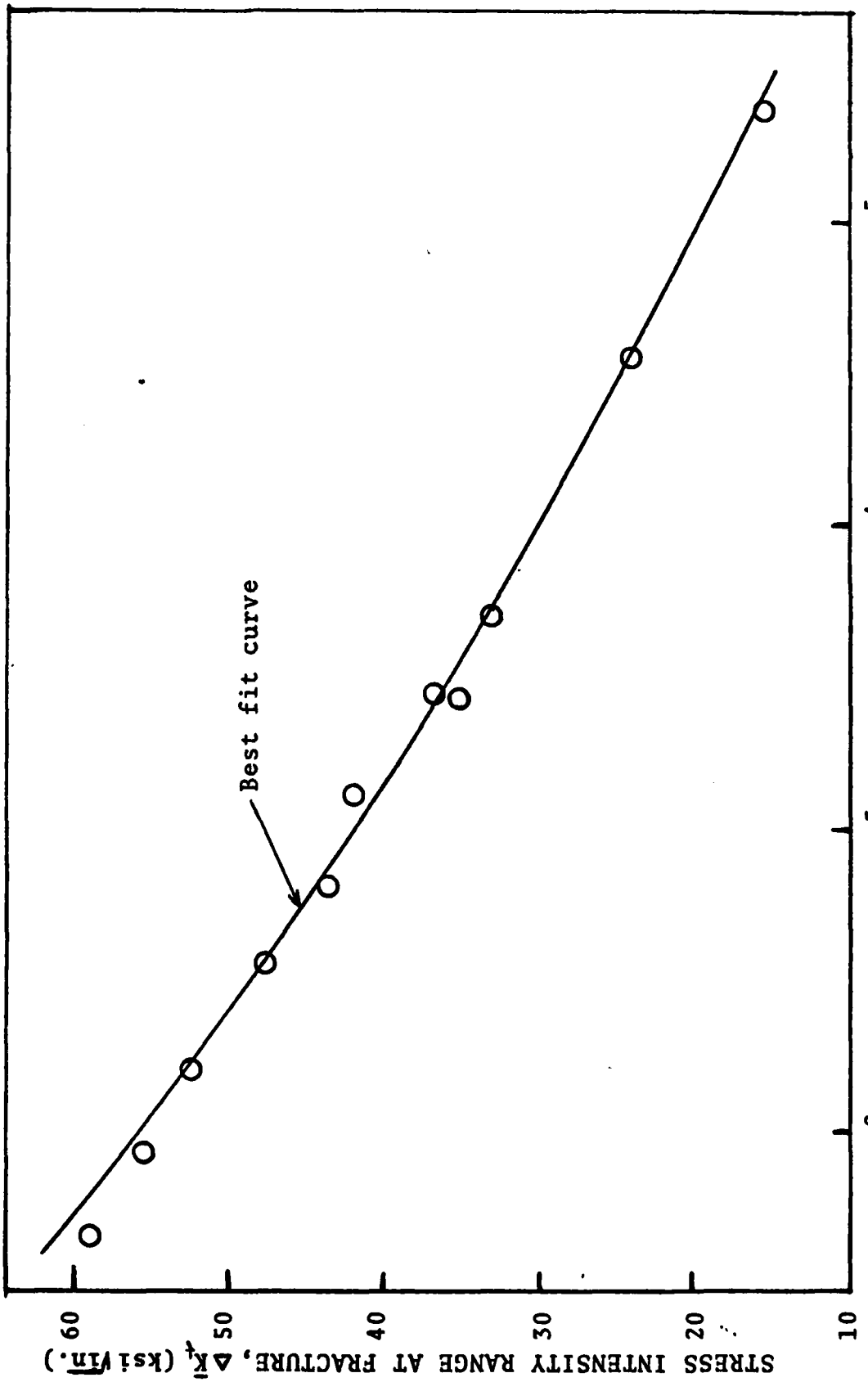

Fig. 6. Variation of stress intensity range at fracture with number of cycles to fracture in 2024-T3 alloy (2a/w = 0.5)

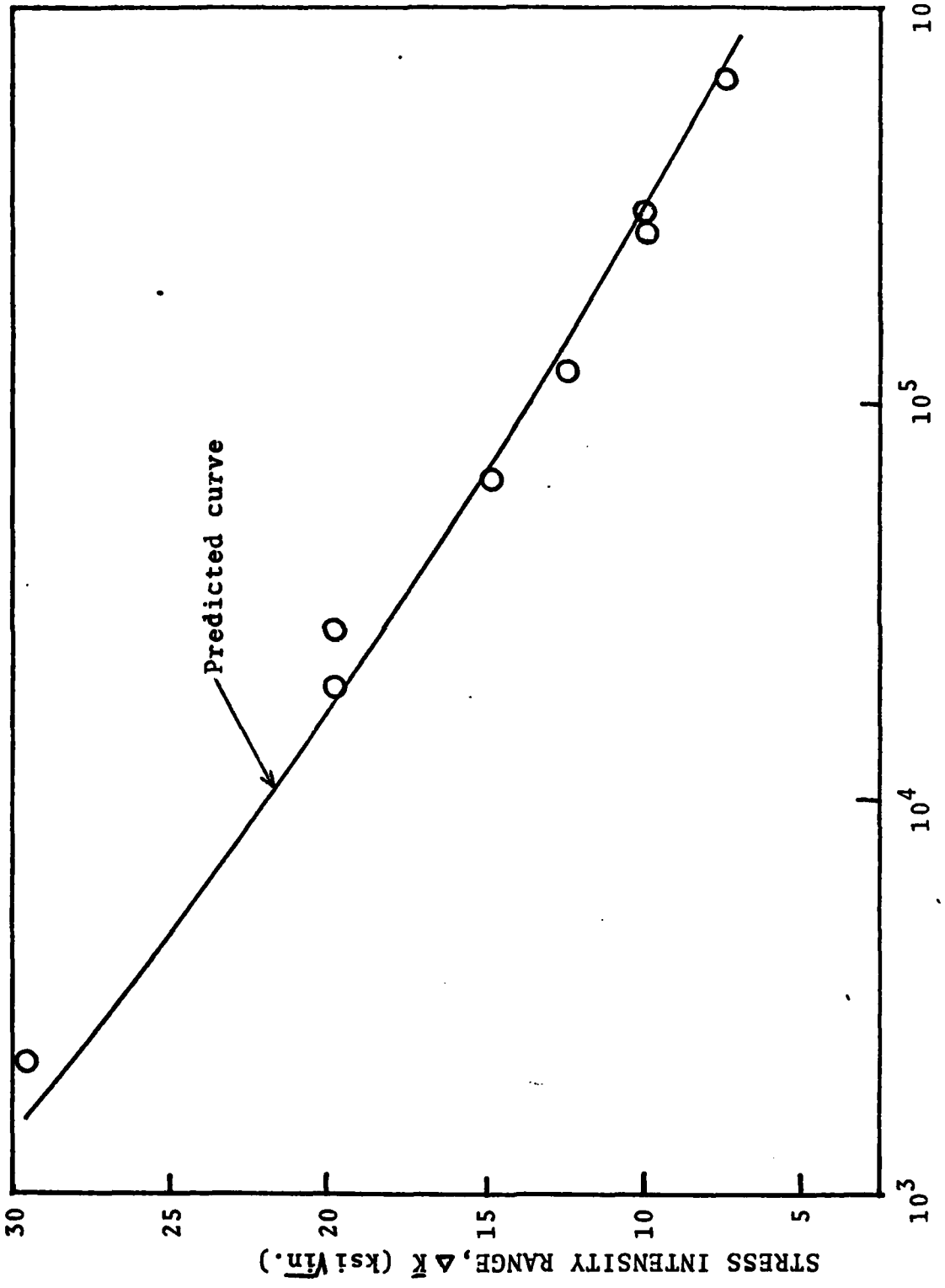

Fig. 7. Variation of stress intensity range with fatigue life in constant amplitude test of 2024-T3 alloy (2a/w =0.5).

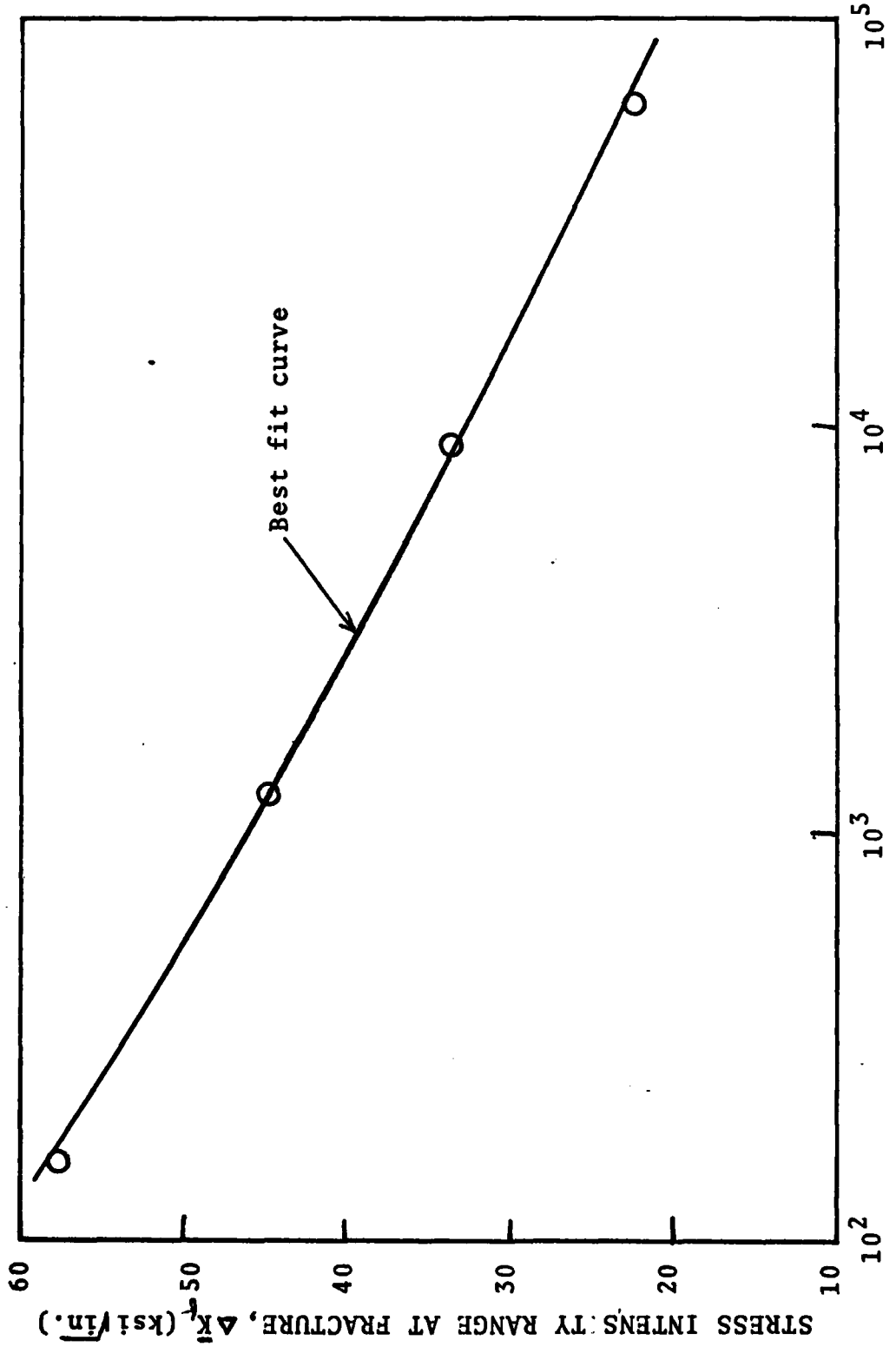

Fig. 8. Variation of stress intensity range at fracture with number of cycles to fracture in 2024-T3 alloy (2a/w = 0.33).

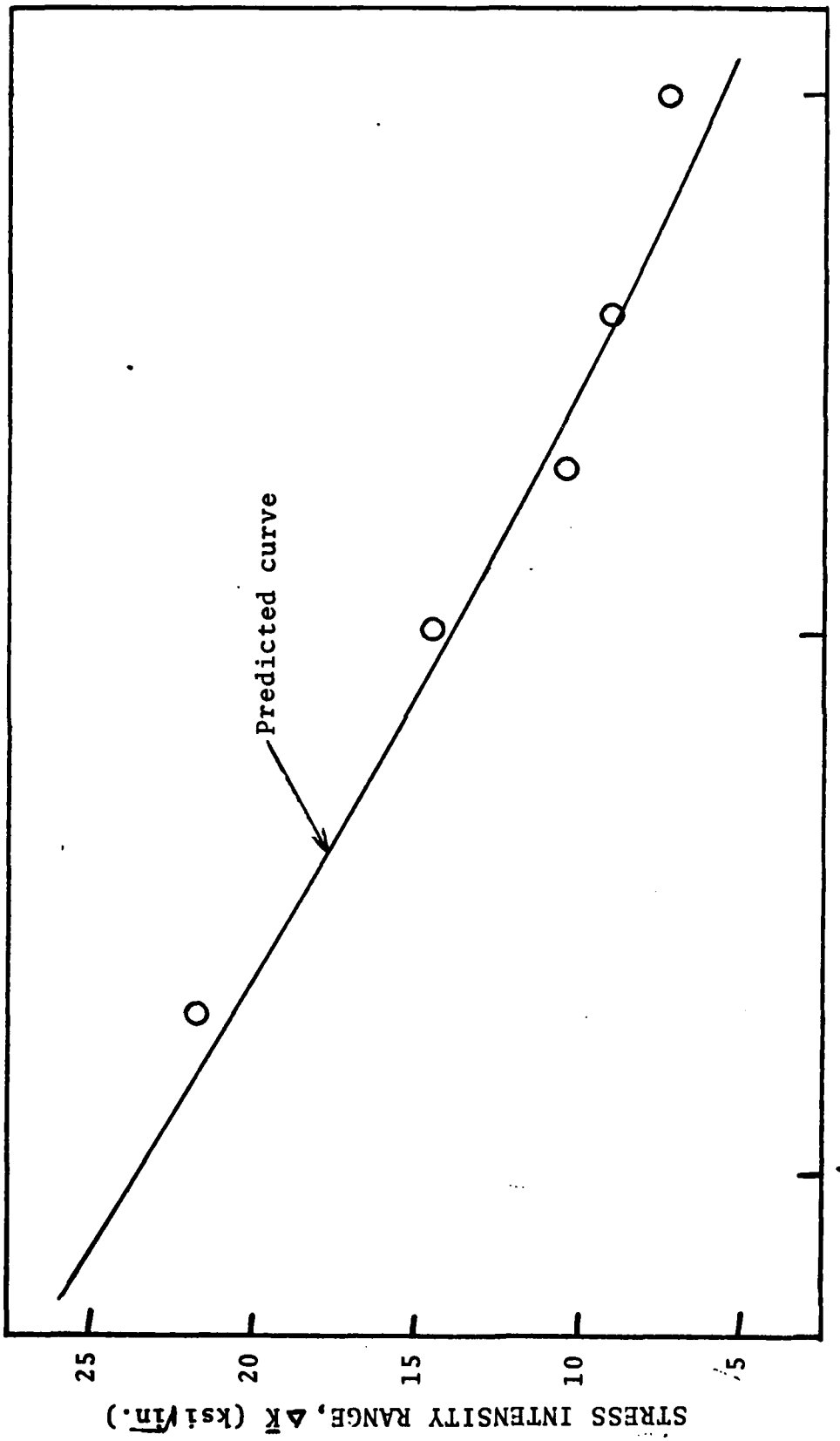

Fig. 9. Variation of stress intensity range with fatigue life in constant amplitude test of 2024-T3 alloy (2a/w = 0.33).

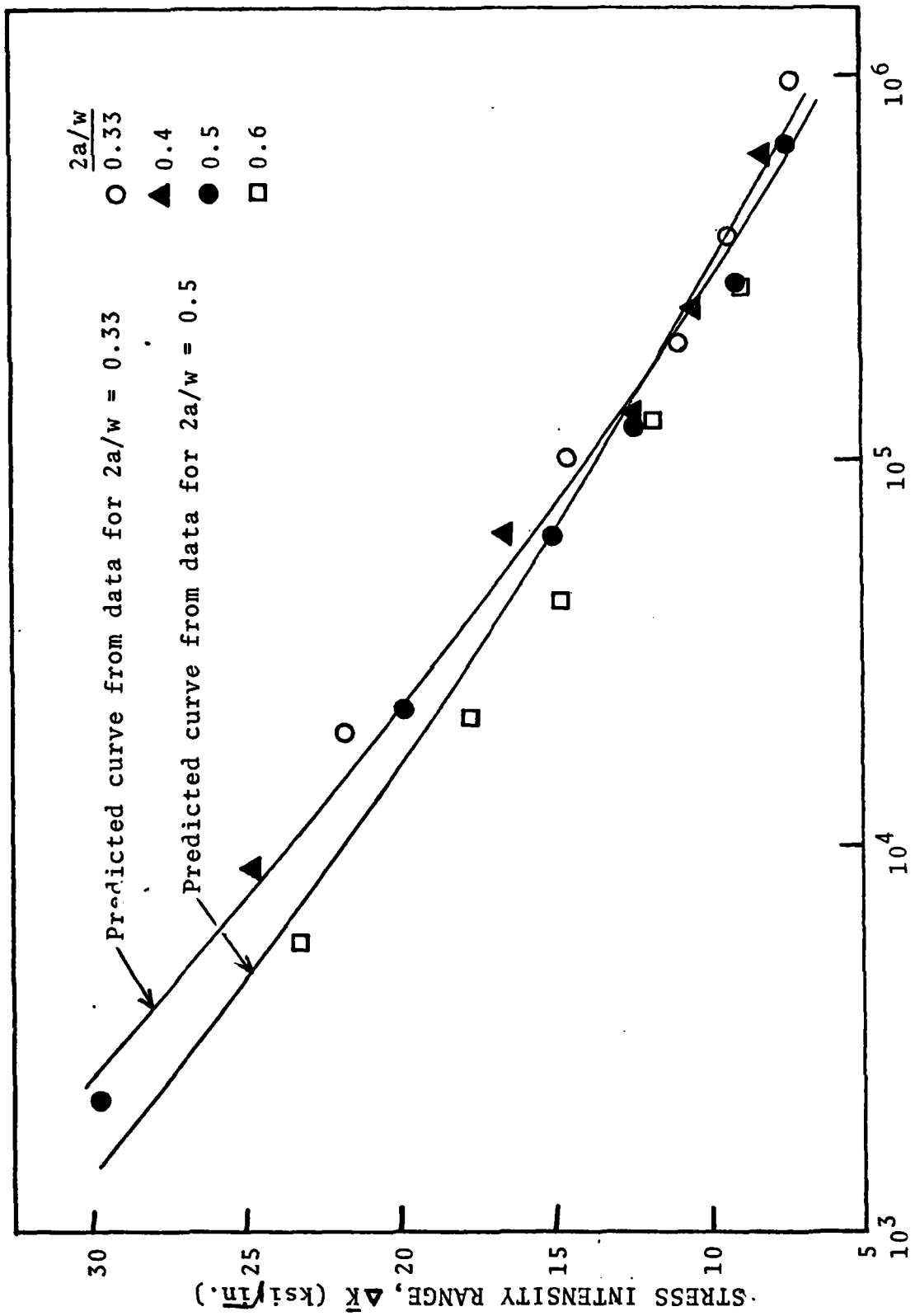

Fig. 10. Stress intensity range as function of fatigue life for different 2a/w values in 2024-T3 alloy and predicted curves from accelerated tests.

cont'd

→ PART B of this related to

EFFECTS OF THICKNESS AND MICROSTRUCTURE ON NONLINEAR TOUGHNESS PARAMETERS ON CORONA-5.

ABSTRACT

The variation of several linear and nonlinear fracture toughness parameters with thickness was studied in CORONA-5 titanium alloy having two different microstructures. The toughness values generally increased with decreasing specimen thickness when the critical point was taken as the maximum load. When the critical point was the onset of subcritical crack growth, the toughness values were essentially independent of thickness. This indicates that either the linear toughness, $\bar{G}_{Io}$, the non-linear energy toughness, $\tilde{G}_{Io}$, or the J-integral toughness, J_{Io}, may be used as a fracture criterion at thickness levels much lower than that required by ASTM Standard E399, if the onset of subcritical crack growth is taken as the critical point.

The microstructure containing fine needles of alpha particles was found to have higher toughness than that containing globular alpha particles. This may be due to the difference in the shape of the particles or in the size of the particles.

INTRODUCTION

The titanium alloy, CORONA-5, is a recently developed α-β alloy which can be heat treated to yield high fracture toughness at moderate strength levels. To obtain a linear fracture toughness value in accordance with the ASTM specification, E399, the thickness of this alloy must be very large, which makes the testing difficult or impractical. Furthermore, for many applications the thickness of the structural members may be lower than those required by ASTM E399, and the linear fracture toughness criterion is not capable of determining the suitability of the material. Several nonlinear fracture toughness criteria have been developed to account for the plasticity in high strength, high toughness materials [1-3]. The usefulness of these criteria for any material will be indicated by their dependence on the geometrical changes in test specimens. The results of a study on the geometry dependence of various non-linear toughness parameters in different alloys have been published [4]. Since CORONA-5 is a potential candidate for structural applications, knowledge of its fracture characteristics in the small thickness range is very important.

In this report the results of an investigation of the thickness dependency of linear as well as nonlinear toughness parameters in CORONA-5 are presented. The nonlinear toughness

parameters investigated include the nonlinear energy, $\tilde{G}_I$, J-integral J_I and crack opening displacement, G_δ, fracture toughness values. These values were compared with linear toughness values, $\bar{G}_I$. The specimens were heat treated to produce two different microstructures. The effect of the change in microstructure on toughness values was also examined.

EXPERIMENTAL PROCEDURE

The material employed for this investigation was received in two batches. The plates received in the first batch were in the low-beta processed condition [Forged at 1800°F (980°C) to 6 in. slab thickness; rolled at 1750°F (955°C) to 3 in. finish thickness]. The first set of specimens was prepared from these plates and was given the following additional heat treatment: 1525°F/4 hr/air cool + 1300°F/6 hr/air cool (Heat Treatment 1). The processing details of the second batch of plates were not available. Hence, the specimens prepared from these plates were annealed for 1 hr at 1725°F (943°C) to transform the material completely to the beta phase and remove all the phase changes induced by earlier processing. It was then subjected to the following additional treatment: 1525°F/4 hr/air cool + 1300°F/6 hr/air cool (Heat Treatment 2). Although the final stages of treatment were the same for both heat treatments, the low-beta processing in Heat Treatment (HT) 1 and beta anneal in HT2 induced great differences in the microstructures.

The thickness dependence of the linear toughness, $\bar{G}_{Ic}$, the nonlinear energy toughness, $\tilde{G}_{Ic}$, the J-integral toughness, J_{Ic} and the COD toughness, $G_{\delta c}$, were determined by testing compact tension specimens with W = 3 in. in the T-L orientation. The specimens and the tests conformed with the ASTM E399 requirements, except for some specimens which had smaller

thicknesses. A batch of specimens varying in thickness from 0.5 in. to 1.5 in. was prepared for each heat treatment. These thicknesses included those above and below the ASTM requirement for plane strain fracture toughness testing, $B \geq 2.5 (K_{Ic}/\sigma_{ys})^2$. The tests were conducted on an MTS servohydraulic system operated in load control.

The specimens with thicknesses lower than the minimum thickness required for plane strain fracture showed significant subcritical crack growth, as evidenced by sudden changes in the slopes of the load-displacement curves. Most of the nonlinearity of the curves occurred after the onset of subcritical crack growth. Two critical points were identified for these specimens: (a) the onset of subcritical crack growth, and (b) the initiation of unstable fracture, which coincided with the maximum load. From an engineering point of view the onset of unstable fracture is more important. However, the analytical bases for most of the nonlinear methods are appropriate only at the onset of subcritical crack growth. Hence, the toughness values were determined from the load-displacement curves at point (a) and at point (b).

The microstructures of the specimens after Heat Treatments (HT) 1 and 2 were studied by optical microscopy. The fracture characteristics were analyzed using a Cambridge Stereoscan scanning electron microscope.

RESULTS AND DISCUSSION

The variation of different fracture toughness parameters as a function of specimen thickness, determined at points (a) and (b) for HT1, are shown in Fig. 1 and 2, respectively. When the onset of subcritical crack growth was taken as the critical point (Fig. 1), $\bar{G}_{Io}$, $\tilde{G}_{Io}$ and J_{Io} were essentially constant at all thicknesses, and the toughness values were close to one another in all tests. When the maximum load was taken as the critical point (Fig. 2) all toughness parameters increased with decreasing specimens thickness. $\tilde{G}_{Ic}$ and J_{Ic} varied in a similar fashion, $\tilde{G}_{Ic}$ being slightly higher than J_{Ic} in all cases. The linear toughness values, $\bar{G}_{Ic}$ were lower than $\tilde{G}_{Ic}$ and J_{Ic}. At both critical points G_{δ} had higher values than the other three parameters and varied more irregularly with thickness. This is probably due to the inaccuracy associated with the determination of the crack opening displacement from a fracture toughness test of compact tension specimens. Where the ASTM minimum thickness criterion was satisfied, the differences between the fracture toughness values at the onset of subcritical crack growth and at the maximum load were negligible and were close to the ASTM standard toughness, G_{Ic}. This was anticipated since the extent of subcritical crack growth was negligible when the plane strain fracture criterion was satisfied.

The average value of the fracture toughness, G_{Ic} obtained in these tests was 332 in lb/in.^{2} corresponding to K_{Ic} = 77.5 ksi$\sqrt{in.}$ This value agrees very well with the toughness value for this heat treatment (K_{Ic} = 76.3 ksi$\sqrt{in.}$) reported by Rockwell International Corporation [5].

The specimens that were given HT2 showed higher toughness, but the variation in toughness values with thickness was similar to those having HT1. At the onset of subcritical crack growth all toughness values were essentially constant (Fig. 3). At peak load, the nonlinear toughness values increased with decreasing thickness, although the linear toughness, $\overline{G}_{Ic}$ remained more or less constant (Fig. 4). The corresponding G_δ values were not determined because of the erratic variation of this parameter observed in earlier test results.

The toughness values of CORONA-5 in the two heat treated conditions are characteristic of their microstructures. After HT1 the elongated beta grain structure produced by the low-beta processing was retained as can be seen in Fig. 5a. The alpha particles were globular in shape, as seen in Fig. 5b. During HT2 the specimens were first annealed above the beta transus, which resulted in completely recrystallized, equiaxed beta grain formation (Fig. 6a). Subsequent aging resulted in formation of long needles of alpha (Fig. 6b). There was precipitation of the alpha phase along the prior beta grain boundaries for both heat treatments. However, in

HT1 the alpha phase was large and discontinuous (Fig. 5b), whereas, in HT2 the α phase was relatively thin but almost continuous (Fig. 6b).

Figs. 7 and 8 show the fracture surfaces of the specimens that were subjected to HT1 and HT2, respectively. The HT1 specimens failed transgranularly (Fig. 7a) and the fracture surface contained equiaxed dimples (Fig. 7b), as can be expected from the ductile beta matrix and globular alpha phase. The HT2 specimens failed along prior beta grain boundaries (Fig. 8a). The fracture in this condition also was ductile and occurred predominantly along the interface between the beta and grain-boundary alpha phase. A typical fracture surface from these specimens is seen in Fig. 8b. The high strength of the matrix, strengthened by fine needles of alpha, and the formation of the continuous alpha phase along the grain boundaries seem to have forced the crack to propagate along the grain boundaries. Other investigators also have found that continuous phase precipitation along grain boundaries decreases the toughness of the alloy [5]. The higher toughness of microstructures similar to HT2 in comparison with HT1 has been attributed to the difference in shape of the alpha particles by Chesnutt et al. [6]. Whether the high toughness of HT2 is due to the needle shape or due to the fine size of the alpha phase has not been proven.

CONCLUSIONS

The applicability of several nonlinear fracture criteria for CORONA-5 specimens in thicknesses lower than that required by ASTM Standard E399 was examined by studying their variation with specimen thickness. Two microstructures were studied. The results show that:

1. When peak load is taken as the critical point, the toughness values increase with decreasing thickness below that required for plane strain fracture.
2. When the critical point is selected to be the onset of stable crack growth, the toughness values are independent of thickness.
3. The toughness values determined at peak load are generally much higher than that at the onset of stable crack growth. For example, the 1 in. thick specimen with HT1 has a nonlinear energy toughness value of 971 in. lb/in.^{2} at peak load and 481 in. lb/in.^{2} at the onset of stable crack growth.
4. The microstructure containing fine needles of alpha was found to yield higher toughness than those containing globular alpha.

REFERENCES

1. J. Eftis, D. L. Jones and H. Liebowitz, Engng. Fract. Mech, Vol. 7, p. 491, 1975.
2. A. A. Wells, Proc. Conf. Crack Propagation, Cranfield, England, p. 210, 1962.
3. J. A. Begley and J. R. Landes, Fracture Toughness, ASTM STP 514, Am. Soc. Test. Mat'ls., 1972.
4. P. K. Poulose, D. L. Jones and H. Liebowitz, A Comparison of the Geometry Dependence of Several Nonlinear Fracture Toughness Parameters, to be Published in Engng. Fract. Mech.
5. G. R. Keller, J. C. Chesnutt, F. H. Froes and C. A. Rhodes, Naval Air Systems Command Report NA-78-917, December 1978.
6. J. C. Chesnutt et al., Fracture, 1977, Vol. 2, p. 195.

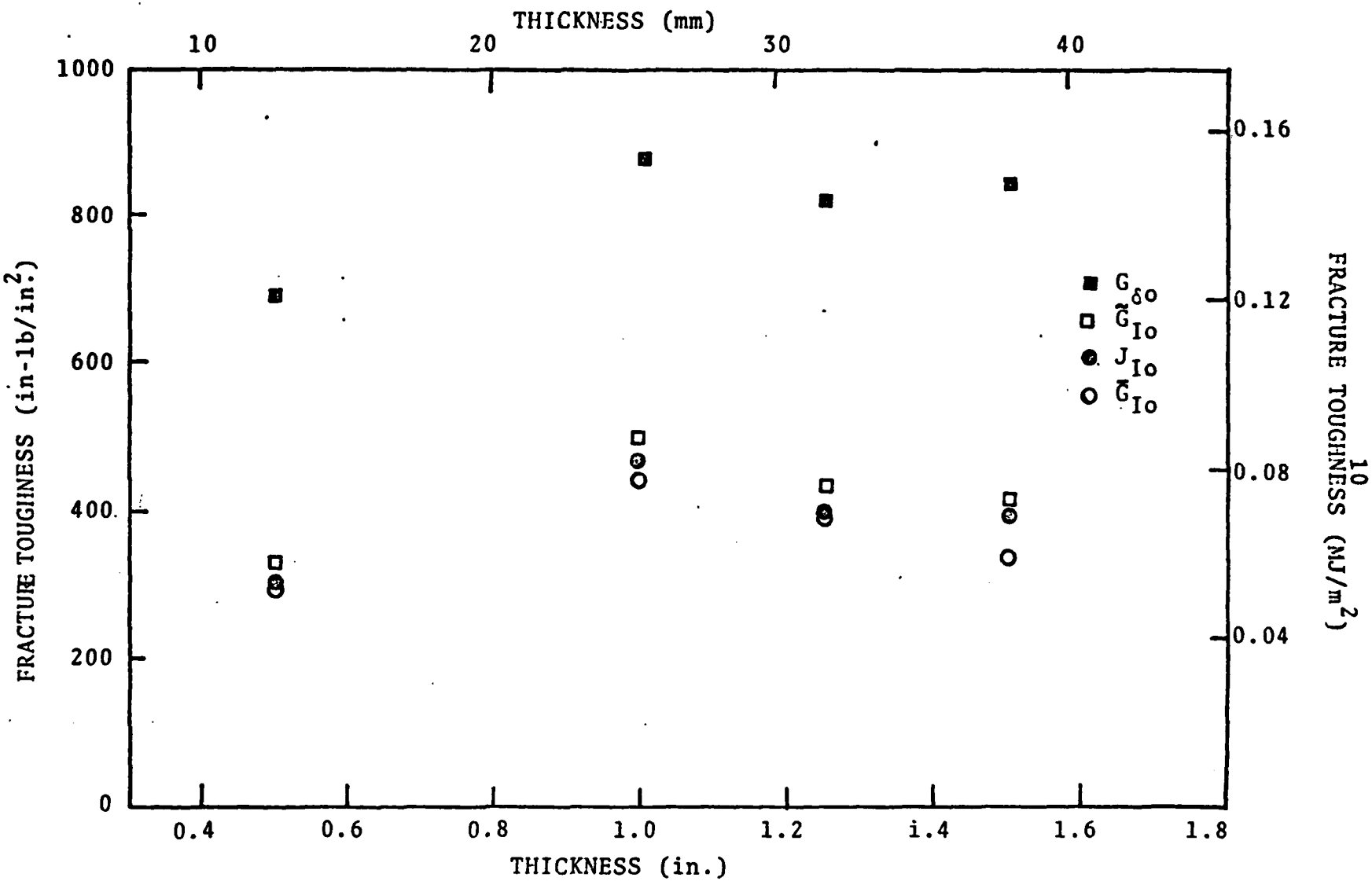

Fig. 1. Variation of toughness patameters with specimen thickness after HT 1 (T-L orientation) determined at the onset of subcritical crack growth.

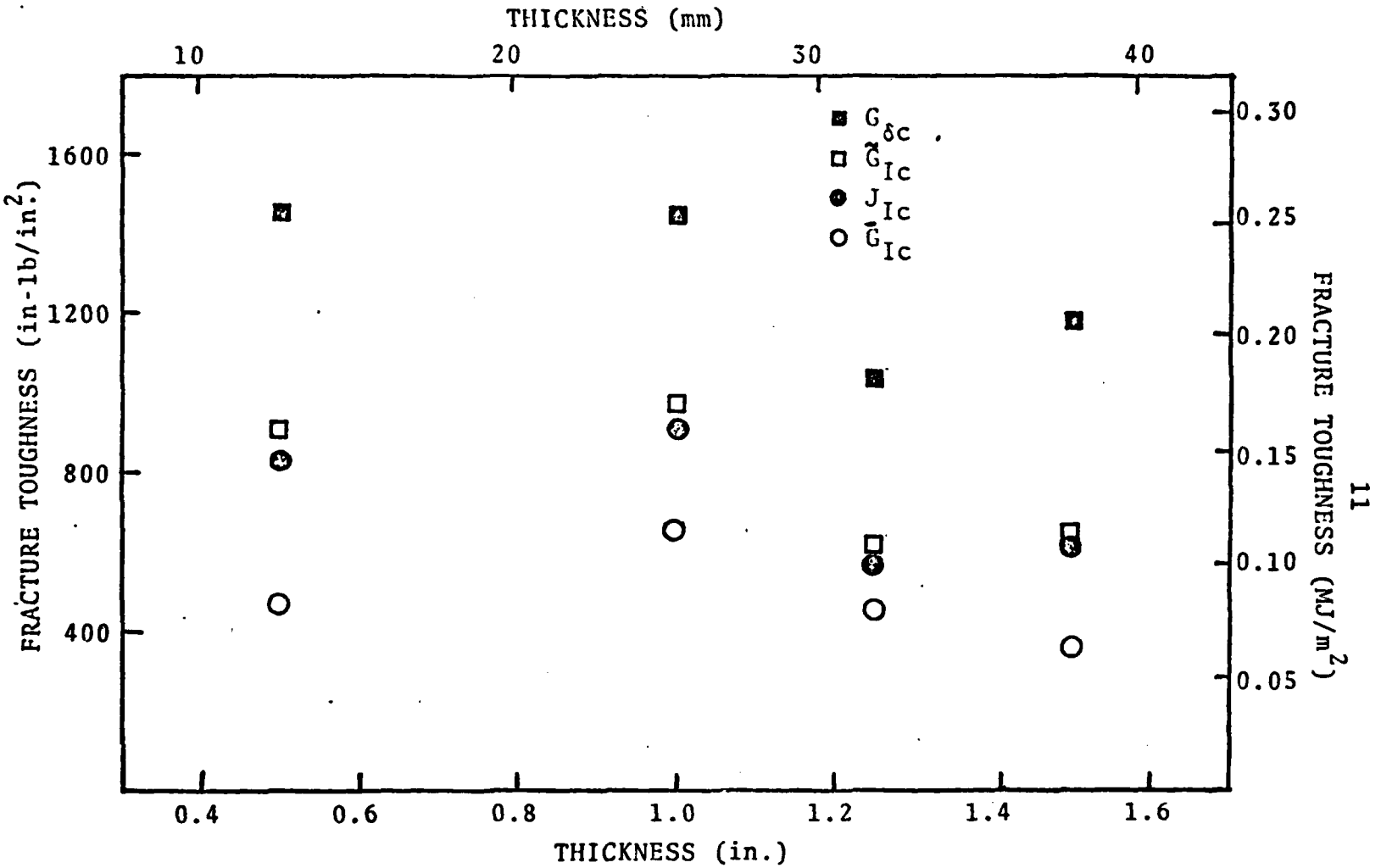

Fig. 2. Variation of toughness parameters with specimen thickness after HT 1 (T-L orientation) determined at peak load.

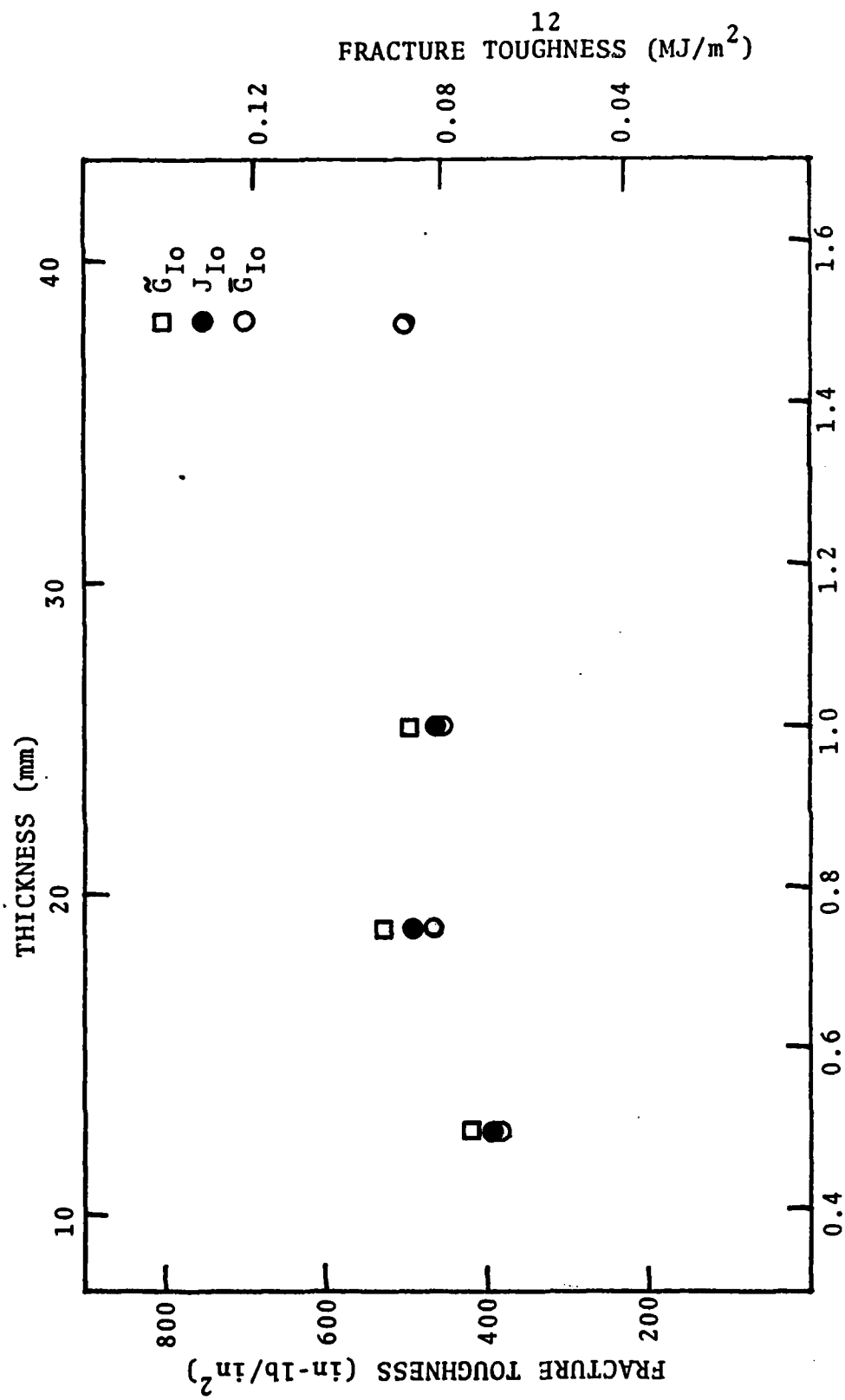

Fig. 3. Variation of toughness parameters with specimen thickness after HT 2 (T-L orientation) determined at the onset of subcritical crack growth.

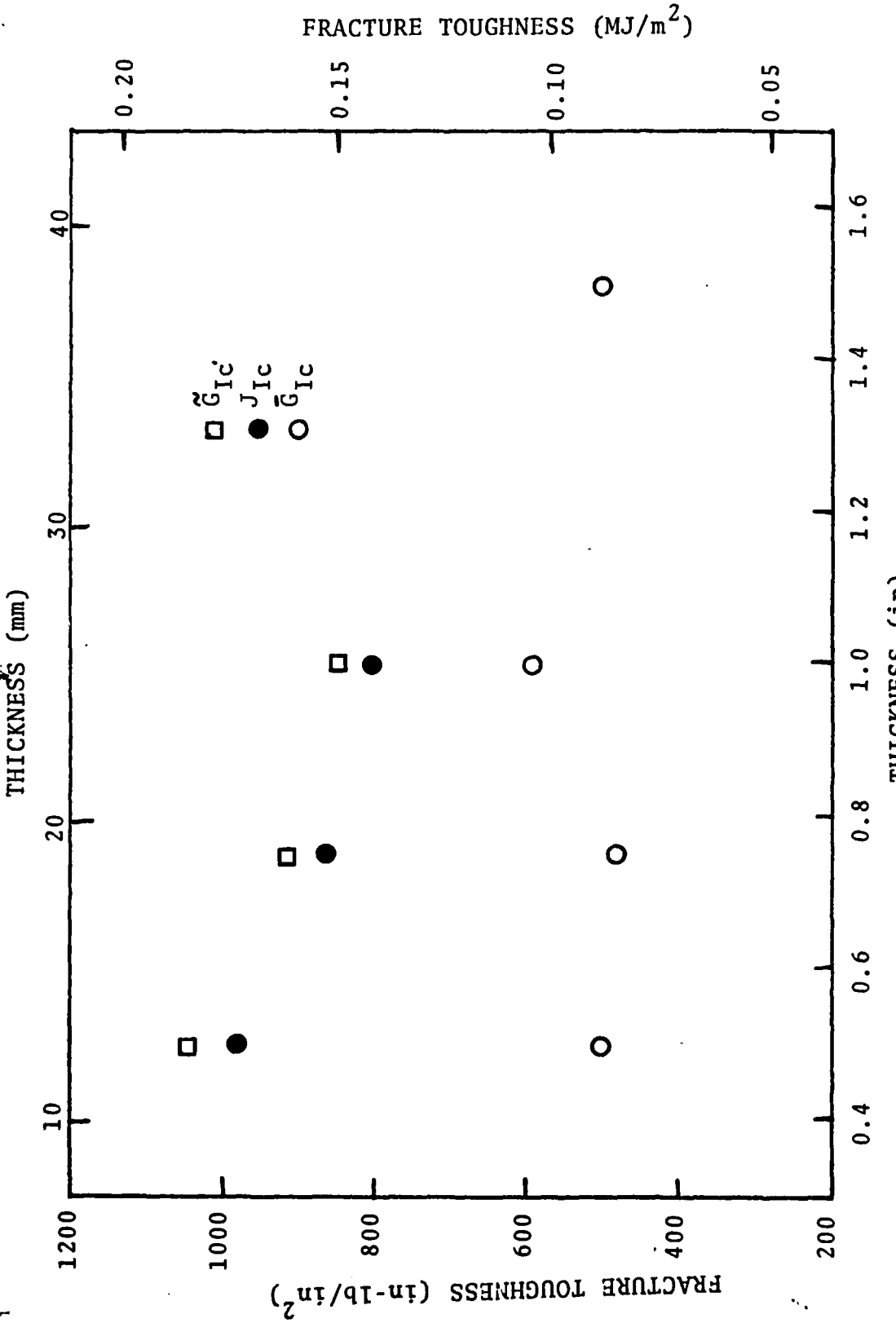

Fig. 4. Variation of toughness parameters with specimen thickness after HT 2 (T-L orientation) determined at peak load.

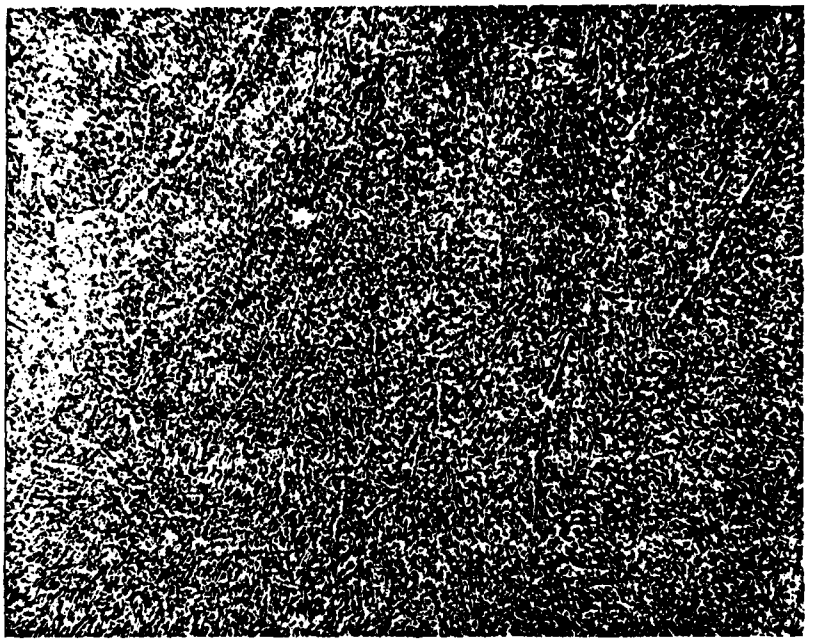

(a)

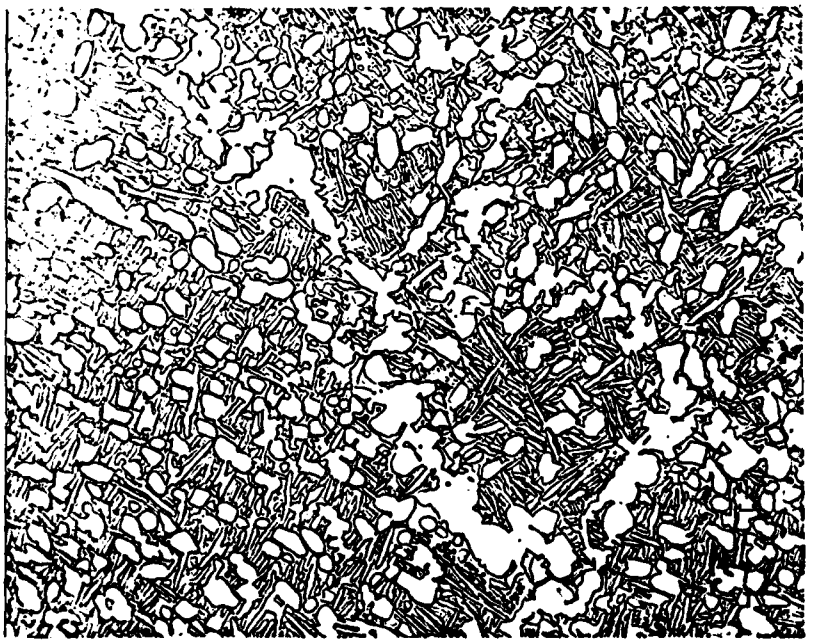

(b)

Fig. 5. Heat treatment 1 (a) Elongated grain structure X50 (b) Globular α in β matrix X500.

(a)

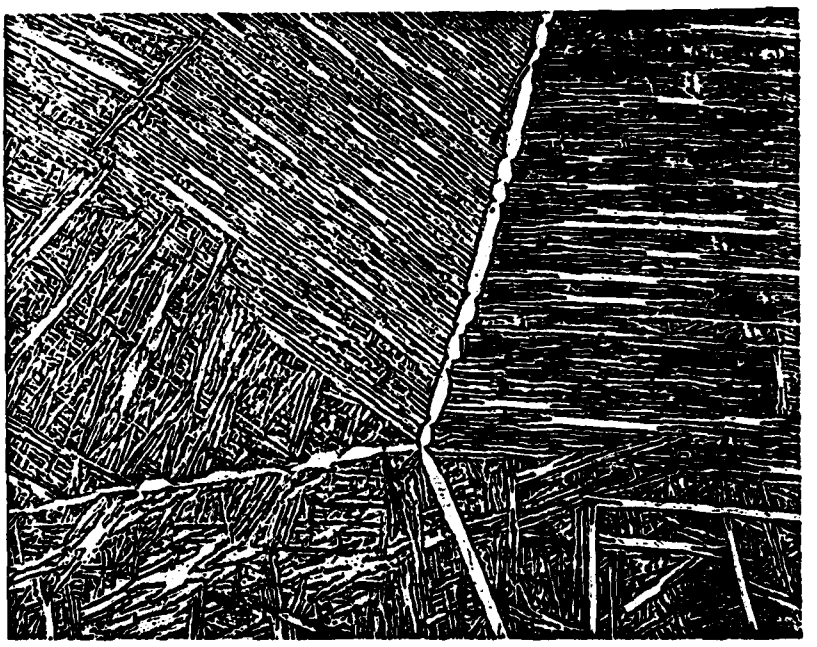

(b)

Fig. 6. Heat treatment 2 (a) Equiaxed grain structure X50 (b) Needle shaped α particles X500.

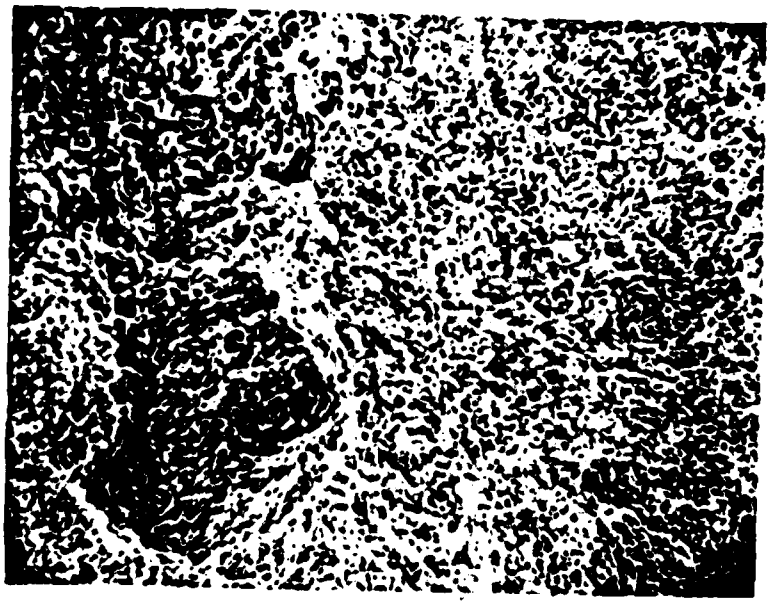

(a)

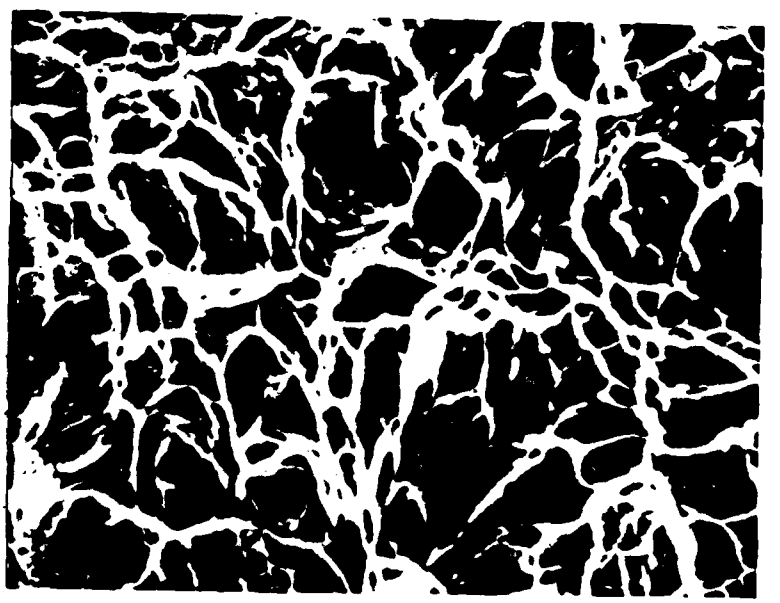

(b)

Fig. 7. Heat treatment 1 (a) Transgranular fracture surface X68 (b) Equiaxed dimples at fracture surface X1350.

(a)

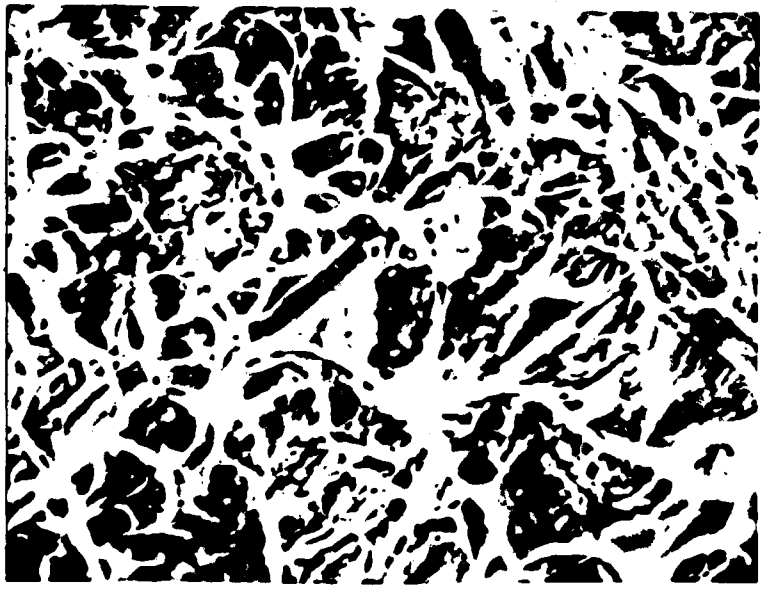

(b)

Fig. 8. Heat treatment 2 (a) Intergranular fracture surface X65 (b) Facets indicating fracture along the α-β interface X1300.

END

FILMED

1-83

DTIC